Quantifying the enhancement mechanisms of surface-enhanced Raman scattering using a Raman bond model

Ran Chen¹ and Lasse Jensen^{1, a)}

Department of Chemistry, Pennsylvania State University, University Park,

Pennsylvania 16802, United States

(Dated: 4 November 2021)

In this work, a Raman bond model which partitions the Raman intensity to interatomic charge flow modulations or Raman bonds is extended from the static limit to frequency dependent cases. The model is based on damped response theory and thus enables a consistent treatment of off-resonance and resonance cases. Model systems consisting of pyridines and silver clusters are studied using time dependent density functional theory to understand the enhancement mechanisms of surface-enhanced Raman scattering (SERS). The Raman bonds in the molecule, the inter-fragment bond, and the cluster are mapped to the enhancement contributions of the molecular resonance mechanism, the charge transfer mechanism, and the electromagnetic mechanism. The mapping quantifies the interference among the coupled mechanisms and interprets the electromagnetic mechanism as charge flow modulations in the metal. The dependence of the enhancement on the incident frequency, the molecule-metal bonding, and the applied electric field is interpreted and quantified. The Raman bond framework offers an intuitive and quantitative interpretation of SERS mechanisms.

a)Electronic mail: jensen@chem.psu.edu

I. INTRODUCTION

Surface-enhanced Raman scattering (SERS) relies on large signal enhancements due to plasmon excitations and has been shown to be able to detect single molecules with high specificity ^{1–7}. SERS has also been extended to other analytic techniques such as tip-enhanced Raman scattering (TERS)^{8–11} which has offered single molecule images with subnanometer resolutions ^{12,13}. The plasmon resonance amplifies the local fields at the surface of metal structures which enhances Raman signals and the mechanism is classified to be electromagnetic (EM)^{14–19}. Other enhancement mechanisms such as the molecule-metal bonding, the charge transfer resonance (CT), and the molecular resonance (RRS) are grouped to be chemical (CM)^{20–27}. Enhancements ranging from 10⁵ to 10¹⁰ can be reached within the gaps between nanoparticles^{28–33}. Classic electrodynamics models show that the EM enhancements increase as the gaps close ^{34–38} but the EM enhancements can decrease when the gap is in the subnanometer scale where quantum mechanical effects such as the spill-out of electrons and tunneling become important ^{39–45}. To correctly interpret SERS enhancements, it is crucial to describe EM and CM consistently especially when CM and EM are both important ^{46–49}. Although we often discuss the two mechanisms separately they are in fact coupled and understanding the synergy between them is important.

To consistently describe EM and CM it is necessary to include quantum mechanical effects using electronic structure methods. ^{26,27,50–58} Most of the studies using electronic structure methods focus on understanding CM using either molecules interacting with metal clusters ^{26,27,50–54} or periodic slabs ^{55–58}. Quantum mechanical methods that incorporate both CM and EM have been used to describe SERS. ^{50,53,54} The cluster models have provided key insights into the SERS enhancement mechanisms but are restricted to small clusters due to the high computational cost. It also remains challenging to determine the relative contributions of the different enhancement mechanisms using electronic structure simulations. One approach is to quantify the contributions of CT, EM, and RRS by the ratios of the enhancements at the charge transfer resonance, the plasmon resonance, and the molecular resonance versus the enhancement at the static limit, respectively ⁵⁰. While this approach is simple it assumes that different types of resonance (molecular, charge-transfer or plasmonic) are well separated in energy and therefore the coupling among different mechanisms is weak. An analysis of the different enhancements has also been done by using an orbital-based partitioning of the Raman intensity into molecule and surface contributions. This work found the largest contributions from the molecule with no significant contributions from the

surface. As is common in orbital-based partitioning schemes the results depends on the origin and on the specific basis set employed and thus care must be taken in the analysis. More recently, a semi-empirical approach based on INDO/SCI has been applied to decompose the enhancements into contributions from CM and EM.⁵⁴ The CM contribution was quantified by neglecting the overlap of orbital integrals between Ag and other elements in the simulations. This approach was used to gain insights into the importance of charge-transfer excitations under external bias but it is hard to be generalized to other electronic structure methods.⁵⁴

Another difficulty in using electronic structure methods to understand SERS is the lack of an intuitive interpretation of EM using fully quantum mechanical methods. EM enhancements are often approximated as $|E|^4$, where E is the local field enhancement 22,59,60 . However, it has been shown theoretically that atomic features on metal nanoparticles can result in highly confined fields where the magnitude of the local field can vary greatly over the space of a few nanometers $^{4,28,61-63}$. For these highly confined fields the electric field gradient can contribute significantly to the enhancement and the traditional selection rules of Raman scattering break down $^{2,64-67}$. Therefore, results obtained using electronic structure methods cannot directly be interpreted in terms of the classical $|E|^4$ enhancement since the small clusters used in the simulations naturally contains such atomic features. The advantage of electronic structure methods is that CM and field gradient effects are fully accounted for in the simulations but it becomes important to develop new ways of interpreting the results.

In this work, we present an a Raman bond model (RBM) for analyzing the frequency dependent Raman spectra of molecules interacting with metal clusters. The model is an extension of a RBM recently proposed to analyze the CM contribution to SERS.⁶⁸ The RBM partitions the Raman intensities into Raman bonds based on interatomic charge flow modulations obtained from a Hirshfeld analysis⁶⁹ of the induced density. Here this model is combined with damped response theory and a short-time approximation to consistently treat off-resonance and resonance Raman simulations.⁷⁰ Using a model system consisting of a pyridine interacting with a Ag₂₀ cluster we show how the Raman bonds in the molecule, the inter-fragment bond, and the metal cluster can be mapped to the enhancement contributions of RRS, CT, and EM. This mapping enables the different enhancement contributions of SERS to be quantified. Furthermore, we show that EM in electronic structure simulations can be interpreted as charge flow modulations in the metal. As a further illustration of this model we use it to interpret how the SERS enhancement mechanisms depend on external electric fields.

II. THEORY

To understand the frequency dependent Raman spectra of molecules interacting with metal clusters we will adopt a time-dependent density functional theory (TDDFT) method, which uses a short-time approximation to evaluate the Raman scattering cross section.^{70,72} This short-time approximation makes it possible to calculate both normal and resonance Raman intensities from the geometrical derivatives of the frequency-dependent (complex) polarizabilities.

RBM partitions the polarizability derivative versus the vibrational mode $\partial \alpha_{ab}/\partial Q_k$ as⁶⁸:

$$\frac{\partial \alpha_{ab}}{\partial Q_k} = \sum_{i} \frac{\partial \left\{ - \int (r_b - R_{i,b}) \delta \rho_{i,a} dr \right\}}{\partial Q_k} + \sum_{ij,j>i} \frac{\partial \left\{ q_{ij,a} (R_{i,b} - R_{j,b}) \right\}}{\partial Q_k} , \qquad (1)$$

where $-r_b$ is the electronic dipole operator in direction b and $R_{i,b}$ is the coordinate of atom i in direction b. $\delta \rho_{i,a}$ is the induced electron density for atom i caused by the external field in direction a, which is calculated adopting Hirshfeld partitioning⁶⁹. $q_{ij,a}$ is the charge flow between atom i and j induced by the external field in direction a, which is calculated adopting Loprop method⁷³. The use of the loprop method ensures that the results is independent of the origin. The first term on the right side of Eq.1 describes the vibrational modulation of the induced atomic electron densities, which corresponds to the atomic contributions to the Raman intensity. The second term on the right side of Eq.1 describes the vibrational modulation of the interatomic charge flows, which corresponds to the bond contributions to the Raman intensity. The bond contributions are dominant and denoted as Raman bonds.

At the static limit, the imaginary parts of the polarizability derivatives are negligible and the atomic and bond contributions are real numbers. When the incident frequency is larger than zero, the atomic and bond contributions are complex and thus the analysis needs to account for both the real and imaginary contributions. To facilitate this we will use that $\partial \alpha_{ab}/\partial Q_k$ can be defined as a vector, $\mathbf{R}^{\text{total}}$, on the complex plane. The Raman intensity is determined by the magnitude of $\mathbf{R}^{\text{total}}$ which we will denoted as p^{total} . Similarly, the atomic and bond contributions can also be defined as vectors \mathbf{R}^{atom} and \mathbf{R}^{bond} , respectively. Interference among the individual Raman atoms and bonds can be characterized by the phases of the Raman vectors. The phases of \mathbf{R}^{atom} and \mathbf{R}^{bond} can vary from -180° to 180° continuously in frequency dependent cases but are discrete (-180° or 180°) at the static limit.

To simplify the analysis, the individual contributions R^{atom} and R^{bond} can be grouped based on their spatial distributions within a SERS model system. In a SERS model system consist-

ing of a molecule and a metal cluster, we showed previously⁶⁸ that it is convenient to group the contributions as $R^{\rm mol}$, $R^{\rm clu}$, and, $R^{\rm inter}$ which corresponds to the molecular, the cluster, and the inter-fragment contributions to the Raman intensity, respectively. Since the individual contributions are additive the following $R^{\rm mol} + R^{\rm inter} + R^{\rm clu} = R^{\rm total}$ is fulfilled. It is important to point out that the Raman intensity is determined by the square of $R^{\rm total}$ and thus there is interference among the individual terms. However, the analysis can be further simplified by projecting the grouped contributions $R^{\rm mol}$, $R^{\rm inter}$, and $R^{\rm clu}$ to the total vector $R^{\rm total}$ as:

$$p^{\text{mol}} = \mathbf{R}^{\text{mol}} \cdot \mathbf{R}^{\text{total}} / p^{\text{total}}$$

$$p^{\text{inter}} = \mathbf{R}^{\text{inter}} \cdot \mathbf{R}^{\text{total}} / p^{\text{total}}$$

$$p^{\text{clu}} = \mathbf{R}^{\text{clu}} \cdot \mathbf{R}^{\text{total}} / p^{\text{total}} ,$$
(2)

where p^{mol} , p^{inter} , and p^{clu} are the group projections that can be used to quantify the contributions of each of the terms. Again, the projection ensures that the contributions are additive and thus $p^{\text{mol}} + p^{\text{inter}} + p^{\text{clu}} = p^{\text{total}}$ is fulfilled.

III. COMPUTATIONAL DETAILS

All calculations in this work were performed using a local version of the Amsterdam density functional (ADF) program package^{74,75}. The Becke-Perdew (BP86) XC-potential^{76,77} and triple- ζ polarized slater type (TZP) basis set with large frozen cores from the ADF basis set library were used. The scalar relativistic effects were accounted for by the zeroth-order regular approximation (ZORA)⁷⁸. For the systems in this work, full geometry optimization and frequency calculations were performed. The vibrational frequencies and normal modes were calculated within the harmonic approximation. Polarizability calculations were performed using the AOResponse module⁷⁰ with the Adiabatic Local Density Approximation (ALDA). The phenomenological damping parameter $\Gamma = 0.004$ a.u. in this work. The Polarizability derivatives were calculated by numerical differentiation with respect to the normal mode displacements. For any system in this work, the molecule-cluster axis was aligned with x-axis and only the xx components in the polarizabilities were considered. All Raman bond figures in this work were plotted using PyMOL⁷⁹.

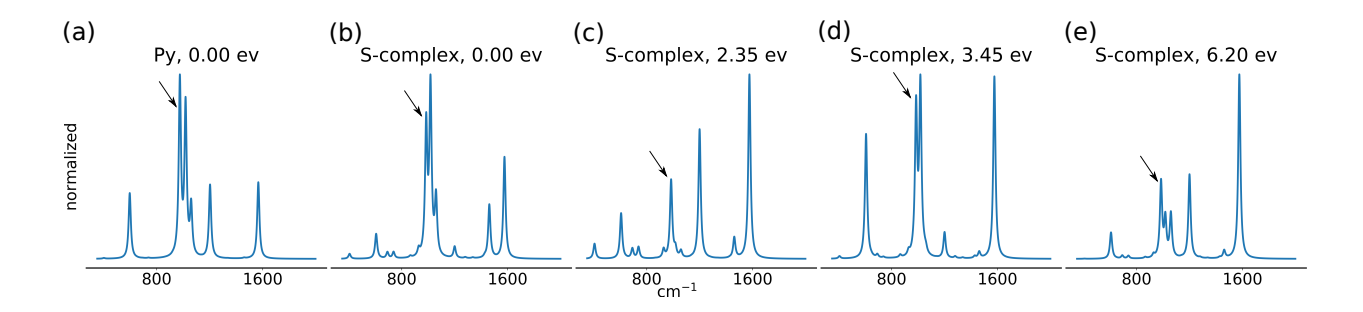


FIG. 1. (a): p^{total} versus the vibrations in the Py at 0.00 eV. p^{total} versus the vibrations in the S-complex (b) at 0.00 eV, (c) at 2.35 eV, (d) at 3.45 eV, and (e) at 6.20 eV. The mode v_1 (974.65 cm⁻¹ in the Py and 984.97 cm⁻¹ in the S-complex) is labeled by the arrow.

IV. RESULTS AND DISCUSSION

To demonstrate how RBM can be used to understand the different enhancement mechanisms of SERS, we will consider a model system consisting of a pyridine molecule (Py) bound to the surface of a tetrahedral Ag₂₀ cluster (S-complex). Previous work has shown that this is a simple model system for understanding the enhancement mechanisms of SERS using first-principles simulations.⁵⁰ In the following we will show how the Raman bond projections p^{mol} , p^{inter} , and p^{clu} can be used to gain insights into the different enhancement mechanisms.

In Fig.1(a) we plot p^{total} of Py versus the vibrations at the static limit. For the S-complex we plot the frequency dependent p^{total} obtained at 0.00 eV, 2.35 eV, 3.45 eV, and 6.20 eV in Fig. 1(b), (c), (d), and (e), respectively. These frequencies have been chosen as they correspond to different types of resonance in the S-complex. The different types of resonance of the S-complex are fairly well separated in energy and the previous work⁵⁰ assumed that the coupling among different mechanisms is weak. At 0.00 eV the S-complex is far from any resonance and we can learn about the SERS mechanism at the static limit which results from changes to the electronic structure of the molecule when adsorbed on the metal cluster.^{19,21,27,51} Previously, we showed how RBM can be used to understand this enhancement mechanism as charge flow modulations across the moleculemetal interface.⁶⁸ In the S-complex the lowest strong charge transfer excitation occurs at 2.35 eV and corresponds to the transition from the highest occupied orbital (HOMO) of the Ag₂₀ to the lowest unoccupied orbital (LUMO) of the Py. Therefore, calculations of the Raman scattering at this energy should probe the enhancement from the charge transfer excitation. However, it is important to note that there are several weaker transitions within the silver cluster around this energy

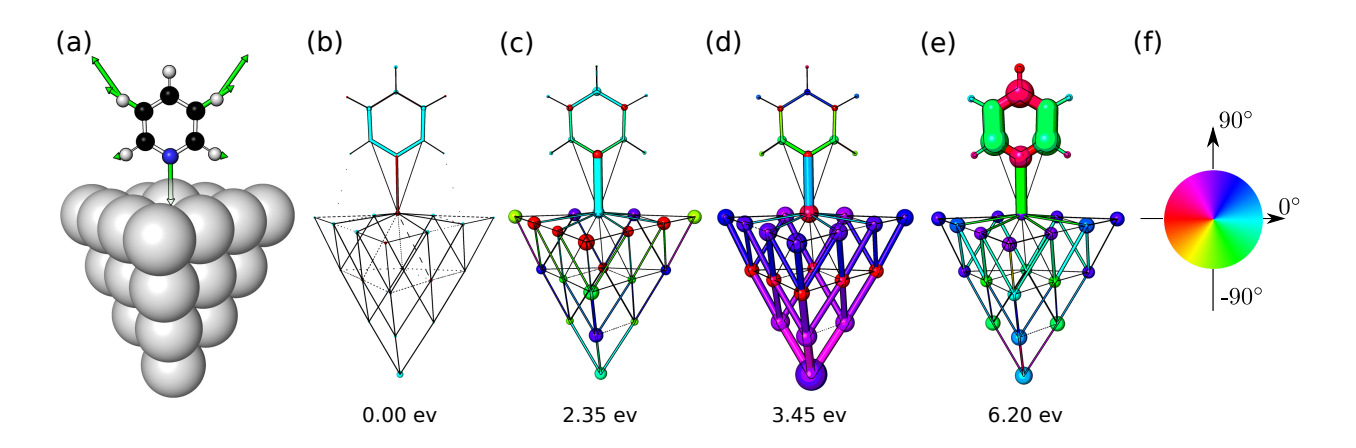


FIG. 2. (a): The vibrational pattern of mode v_1 in the S-complex is shown. R^{atom} and R^{bond} of mode v_1 in the S-complex are plotted at (b): 0.00 eV, (c): 2.35 eV, (d): 3.45 eV, and at (e): 6.20 eV. (f): The color scheme for the phases of R^{atom} and R^{bond} is shown.

which also could contribute to the enhancement. The strong transitions in the silver cluster are located around 3.45 eV and correspond to a superposition of many single-particle transitions and thus plasmon-like in nature. It is therefore expected that the excitation of these strong transitions in the silver cluster will reflect the EM mechanism. Finally, a strong molecular transition in the Py is located at 6.20 eV and calculations of the Raman scattering at this energy should be able to probe the RRS mechanism.

As shown in Fig.1 the Raman spectrum of the S-complex depends strongly on the incident frequency used in the simulations. At the static limit, we see that the mode at 1462.04 cm⁻¹ is strongly enhanced when the Py is adsorbed on the cluster. Also, the relative intensities of the two ring-breathing modes around 1000 cm⁻¹ are reversed. Going on resonance with the charge transfer excitation leads to more significant spectral changes. In particular, the two strongest modes are now the modes at 1200.11 cm⁻¹ and 1576.60 cm⁻¹ instead of the two ring-breathing modes that are normally characteristic of the Raman spectrum of pyridine. At the strong cluster excitation, the ring breathing modes are enhanced, and the Raman spectrum of the S-complex is dominated by four modes at 606.76, 984.97, 1017.45, and 1576.60 cm⁻¹. Finally, at the molecular resonance at 6.20 eV, the Raman spectrum looks similar to the Raman spectrum at the charge transfer resonance, although there are differences in the spectra particularly around the ring-breathing modes. The fact that these two spectra are similar is expected since they both involve excitations into the LUMO of Py.

To understand the enhancements and the spectral changes at different frequencies we will focus

on the v_1 ring breathing mode which is strong at all frequencies. The Raman enhancement for this mode is a factor of 4 at the static limit, around a factor of 60 at the charge transfer resonance, around a factor of 7000 on resonance with the strong silver transitions, and about a factor of 2000 around the pyridine excitation. To explain the dependence of the enhancement on the incident frequency we can use the RBM partitioning. The vibrational pattern of mode v_1 in the S-complex is shown in Fig. 2(a). \mathbf{R}^{atom} and \mathbf{R}^{bond} at the static limit, the charge transfer resonance, the cluster resonance, and the molecular resonance are plotted in Fig. 2(b), (c), (d), and (e), respectively. The phases of \mathbf{R}^{atom} and \mathbf{R}^{bond} are color coded using the color scheme shown in Fig. 2(f). The magnitudes of \mathbf{R}^{atom} and \mathbf{R}^{bond} are represented by the volumes of spheres and cylinders respectively. Although all \mathbf{R}^{bond} and \mathbf{R}^{atom} are calculated and considered in the quantitative analysis, to keep the Raman bond plots in Fig. 2 clear, only the largest 70 \mathbf{R}^{bond} are plotted. All \mathbf{R}^{atom} are plotted.

At the static limit, the small enhancement is explained by the weak Raman bonds in the cluster. The weak molecule-metal bonding in the S-complex does not effectively connects the charge flows across the molecule-metal interface and the charge flows in the cluster cannot respond effectively to the charge flow modulations in the molecule. At the charge transfer resonance, the Raman bonds outside of the molecule, especially the inter-fragment Raman bond are enhanced. The charge flow in the inter-fragment bond is enhanced at the charge transfer resonance and better connects the charge flows across the molecule-metal interface. The charge flows outside of the molecule can respond more effectively to the charge flow modulations in the molecule. At the cluster resonance, the Raman bonds in the cluster are drastically enhanced. The charge flows in the cluster are enhanced drastically due to the cluster resonance and respond much more to the charge flow modulations in the molecule. At the molecular resonance, the Raman bonds in the molecule are predominantly enhanced. The charge flows in the molecule are enhanced due to the molecular resonance, which leads to more charge flow modulations. The enhancement is the largest at the cluster resonance, which indicates that the polarizability of the cluster serves as a large reservoir of charge flows and a large enhancement can be obtained if the vibration manages to modulate the charge flows in the cluster.

By applying the interpretation constructed above to other vibrations, RBM is able to explain SERS selection rules. In the S-complex at the static limit, the charge flows outside of the molecule do not respond effectively to the charge flow modulations in the molecule due to the poor charge flow connectivity, which explains the minor change of the spectral signatures in Fig. 1(b) compared with Fig. 1(a). At specific resonance conditions, the vibrations which can effectively modu-

late the most enhanced charge flows will have large Raman intensities. Thus the spectral signatures change significantly in Fig. 1(c), (d), and (e) compared with Fig. 1(a). Some vibrations such as mode v_{8a} (1576.60 cm⁻¹ in the S-complex) modulate the charge flows more globally and thus gain extra intensities over other modes at resonance conditions.

The Raman bond patterns shown in Fig. 2 at different frequencies generally reflect the different enhancement mechanisms of SERS based on the types of resonance involved. Maybe the most interesting case is on resonance with the silver transitions. Here, the Raman bonds in the cluster are the largest and largely in phase, reflecting the large Raman enhancement at this frequency. The enhancement at the cluster resonance is usually related to the contribution of EM, which is interpreted using classic electrodynamics as the amplified local field amplifying the polarizability derivative of the molecule. Therefore, it is not obvious how the large Raman bonds in the cluster are related to the enhanced local field typically associated with the EM mechanism. To understand this further, we will consider a simple model for the EM enhancement of SERS that consists of treating the molecule and the nanoparticle as two polarizable dipoles.^{21,59} The total polarizability for such a system parallel to the molecule-nanoparticle axis is given by

$$\alpha_{\parallel}^{\text{total}} = \frac{\alpha^{\text{M}} + \alpha^{\text{NP}} + 4\alpha^{\text{M}}\alpha^{\text{NP}}/R^3}{1 - 4\alpha^{\text{M}}\alpha^{\text{NP}}/R^6} , \qquad (3)$$

where $\alpha^{\rm M}$ and $\alpha^{\rm NP}$ are the isotropic polarizabilities of the molecule and the nanoparticle respectively. R is the separation distance between the molecule and the nanoparticle. It should be noted that in this model the chemical bonding between the molecule and the nanoparticle is not included. Thus the polarizability of the inter-fragment bonds is not considered in Eq.3 and charge-transfer between the two subsystems is neglected. The polarizability derivative versus the vibrational mode Q_k is:

$$\frac{\partial \alpha_{\parallel}^{\text{total}}}{\partial Q_k} = \frac{\partial \alpha^{\text{M}}}{\partial Q_k} \frac{(1 + 2\alpha^{\text{NP}}/R^3)^2}{(1 - 4\alpha^{\text{NP}}\alpha^{\text{M}}/R^6)^2} , \qquad (4)$$

where the factor scaling $\partial \alpha^{\rm M}/\partial Q_k$ can be denoted as $|E_{\parallel}|^2$ which is the squared local field enhancement in the parallel direction if the image field contribution in the denominator is ignored.²¹ The Raman intensity is proportional to the squared total polarizability derivative, which leads to the familiar $|E|^4$ enhancement factor.

Alternatively, the polarizability in Eq.3 can be partitioned as:

$$\alpha_{\parallel}^{\text{total}} \approx \alpha^{\text{M}} + \alpha^{\text{NP}} + (4\alpha^{\text{M}}\alpha^{\text{NP}}/R^3)(\frac{V^{\text{M}}}{V^{\text{M}} + V^{\text{NP}}} + \frac{V^{\text{NP}}}{V^{\text{M}} + V^{\text{NP}}})$$
, (5)

where $V^{\rm M}$ and $V^{\rm NP}$ are the volumes of the molecule and the nanoparticle, respectively. Here, we have neglected the denominator in Eq.3 which accounts for the image field effect.²¹ The term $4\alpha^{\rm M}\alpha^{\rm NP}/R^3$ describes the interaction between the molecule and the nanoparticle, which is partitioned based on the relative volumes of the molecule and the nanoparticle. This partitioning based on the volumes of the fragments is consistent with Hirshfeld partitioning used in RBM.

Effective polarizabilities of the molecule and the nanoparticle can then be defined as:

$$\begin{split} \alpha_{\rm eff}^{\rm M} &= \alpha^{\rm M} + (4\alpha^{\rm M}\alpha^{\rm NP}/R^3)(\frac{V^{\rm M}}{V^{\rm M}+V^{\rm NP}})\\ \alpha_{\rm eff}^{\rm NP} &= \alpha^{\rm NP} + (4\alpha^{\rm M}\alpha^{\rm NP}/R^3)(\frac{V^{\rm NP}}{V^{\rm M}+V^{\rm NP}}) \ . \end{split} \tag{6}$$

In this way we can write the polarizability derivative as:

$$\frac{\partial \alpha_{\parallel}^{\text{total}}}{\partial Q_k} \approx \frac{\partial \alpha_{\text{eff}}^{\text{M}}}{\partial Q_k} + \frac{\partial \alpha_{\text{eff}}^{\text{NP}}}{\partial Q_k} \quad , \tag{7}$$

where the first term on the right side can be mapped to R^{mol} and the second term can be mapped to R^{clu} in RBM. Since the partitioning is based on the relative volumes of the two subsystems, the second term will dominate the response. Therefore, we can see that when there is no charge transfer we can map the EM mechanism onto R^{clu} in RBM. At the cluster resonance, R^{clu} or $\partial \alpha_{\text{eff}}^{\text{NP}}/\partial Q_k$ is dominant and thus the amplified local field can be interpreted as the Raman bonds induced in the cluster.

Because EM also contributes to the enhancements at other incident frequencies, the Raman bonds in the cluster can be mapped to and quantify the contributions of EM at other incident frequencies even when the Raman bonds in the cluster are not dominant. However, we should note that the Raman bonds in the cluster can also be induced by the charge transfer between the molecule and the cluster. The Raman bonds in the cluster can only be mapped directly to the local field when the charge transfer is small. As the Raman bonds in the cluster are mapped to the contribution of EM, the Raman bonds in the molecule and the inter-fragment bond can also be mapped to the contributions of RRS and CT. The mapping is consistent with the Raman bond patterns shown in Fig. 2 that the most enhanced Raman bonds at the molecular resonance, the charge transfer resonance, and the cluster resonance are the Raman bonds in the molecule, the inter-fragment bond, and the cluster respectively.

Although, the figures showing the Raman bonds and atoms provide an intuitive illustration of the SERS mechanisms, the main advantage of RBM is the ability to quantify the individual

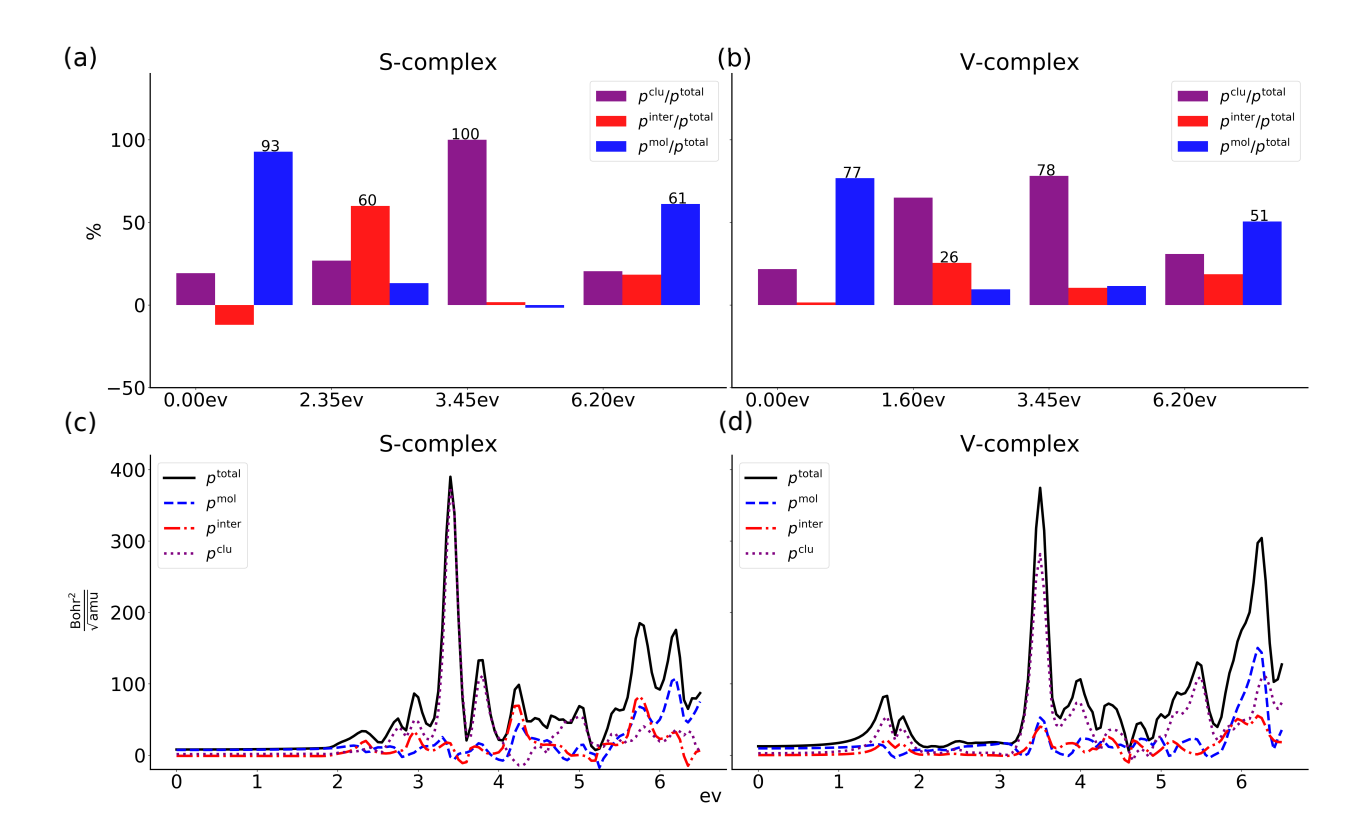


FIG. 3. The percentages of p^{mol} , p^{inter} , and p^{clu} at select incident frequencies are shown in (a) for v_1 in the S-complex, and in (b) for v_1 in the V-complex. The contributions p^{mol} , p^{inter} , and p^{clu} of mode v_1 versus the incident frequency for (c) the S-complex and (d) the V-complex.

contributions to the enhancements. To illustrate this we will quantify the dependence of the enhancement on the molecule-metal bonding. A model system which consists of a pyridine binding on the vertex of a tetrahedral Ag_{20} cluster (V-complex) is compared with the S-complex. The N-Ag bond length is shorter in the V-complex than in the S-complex and thus the charge flows in the V-complex are better connected across the molecule-metal interface. The percentages of p^{mol} , p^{inter} , and p^{clu} of mode v_1 in the S-complex and the V-complex are shown in Fig. 3(a) and (b), respectively.

For the S-complex, this analysis shows that CT contributes 60% of the enhancement at the charge transfer resonance, EM contributes 100% of the enhancement at the cluster resonance, and RRS contributes 61% of the enhancement at the molecular resonance. This is consistent with the Raman bond pictures discussed above, but also highlights the interference among the different enhancement mechanisms. In the V-complex, the charge transfer resonance shifts to 1.60 eV due to the better charge flow connectivity. The RRS contribution decreases from 61% to

51% at the molecular resonance or from 93% to 77% at the static limit. At the charge transfer resonance, the CT contribution decreases from 60% to 26%. The lower RRS or CT contribution is due to the stronger mixing of the molecular states with the cluster states, which results in a stronger contribution of the Raman bonds in the cluster. Likewise, at the cluster resonance, the EM contribution decreases from 100% to 78% due to this increased coupling. The reason is that the better charge flow connectivity in the V-complex enables the charge flows across the system to respond more effectively to the local charge flow modulations induced by the molecular vibration. This in turn reflects that in the V-complex the Raman bonds are enhanced across the whole system whereas the Raman bonds are enhanced more locally in the S-complex.

The enhancements at other incident frequencies can also be interpreted as the interference among RRS, CT, and EM, rather than explained based on the resonance at discrete frequencies. p^{mol} , p^{inter} , and p^{clu} of mode v_1 in the S-complex and V-complex are plotted versus the incident frequency from 0 eV to 6.50 eV in Fig. 3(c) and (d) respectively. The continuous change of the enhancement versus the incident frequency is interpreted by the evolution of the Raman bond pattern, which is simplified as the profile of the three components p^{mol} , p^{inter} , and p^{clu} . The profile of the three components in the S-complex or V-complex forms a platform in the low frequency range until the charge transfer resonance is excited. The peaks corresponding to the charge transfer resonance (CT peaks) are around 2.35 eV for the S-complex and 1.60 eV for the V-complex. The largest enhancement is obtained when the cluster resonance is excited. The peaks corresponding to the cluster resonance (EM peaks) are around 3.40 eV for the S-complex and 3.50 eV for the V-complex. The profile fluctuates in the high frequency range and a large enhancement is obtained when the molecular resonance is excited. The peaks corresponding to the molecular resonance (RRS peaks) are around 6.20 eV for the S-complex and 6.25 eV for the V-complex.

An interesting point is that although the overall enhancements at the cluster resonance are similar for the two complexes, the contribution of $p^{\rm clu}$ is smaller in the V-complex as compared to the S-complex. This indicates that the EM contribution decreases when the charge flow connectivity across the molecule-metal interface is improved. The drop in the EM contribution as the charge-flow connectivity increases is consistent with the reduction of the local field in nanoparticle dimers with very small gaps. 40,44,45 The overall enhancement stays similar because $p^{\rm mol}$ and $p^{\rm inter}$ are larger in the V-complex than the S-complex, which indicates that the CM contribution becomes more significant due to the better charge flow connectivity and compensates the reduction of the EM contribution. Therefore, a reduction in the EM contribution does not necessarily mean

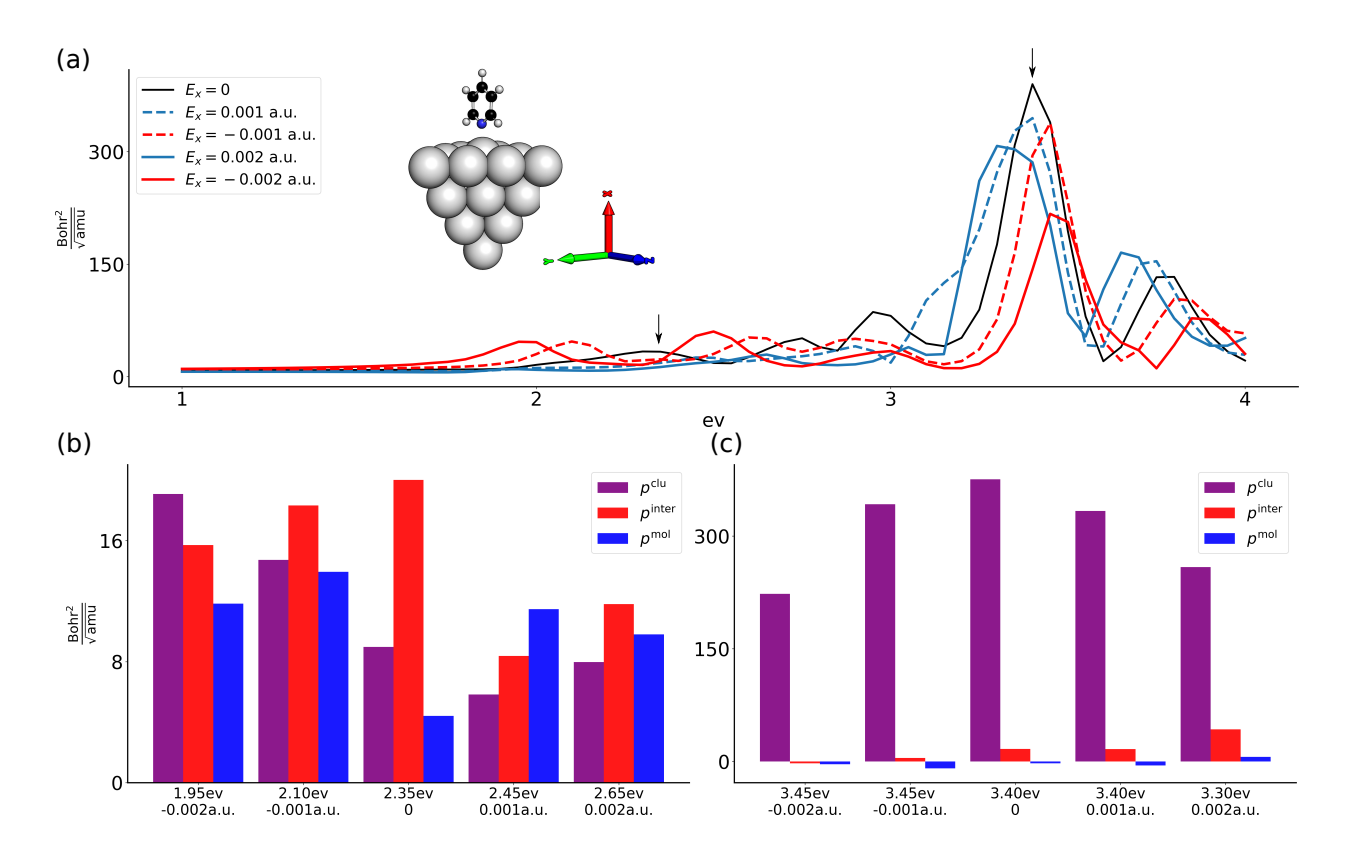


FIG. 4. (a): p^{total} of mode v_1 in the S-complex is plotted versus the incident frequency under different electric fields. The peaks corresponding to the charge transfer resonance and the cluster resonance under no electric field are labeled with arrows. (b): p^{mol} , p^{inter} , and p^{clu} for the CT peaks under different electric fields. (c): p^{mol} , p^{inter} , and p^{clu} for the EM peaks under different electric fields.

a reduction in the Raman intensity which could explain the increased Raman intensities seen in single-molecule TERS with very small tip-molecule separations. 12,13

As an additional application of RMB we will quantify the dependence of the enhancement on external electric fields. Historically, external bias has been used to examine the role of charge-transfer resonance in SERS. $^{81-83}$ The SERS relative intensities being a function of electric bias has often been interpreted as the electric bias tuning the charge transfer resonance frequency. $^{52-54,58}$ The recent TERS studies have renewed the interest in understanding how the SERS enhancement mechanisms depend on external bias. 52,54 In Fig. 4(a) we plot p^{total} of mode v_1 in the S-complex as a function of the incident frequency under different electric fields. The electric fields are applied in x direction, which is along the molecule-metal axis. The positive direction is from the cluster to the molecule. The effect of electric fields on the geometry or the vibrational pattern is not considered. At the ground state, when no electric field is applied, charge (0.056 e) transfers from

the pyridine to the cluster. The negative fields allow less charge to transfer while the positive fields allow more charge to transfer from the pyridine to the cluster. We find that the CT peak is red shifted by the negative fields and blue shifted by the positive fields. The Raman intensity at the CT peak is enhanced by the negative fields and reduced by the positive fields. The individual contributions to the Raman intensities at the CT peaks under different electric fields are plotted in Fig. 4(b). At the charge transfer resonance, compared with the Raman intensity under no electric field, the larger enhancements under the negative fields can be explained by the increases of p^{clu} and p^{mol} . Meanwhile, the smaller enhancements under the positive fields are explained by the reduced p^{clu} and p^{inter} . By perturbing the charge transfer by a small amount, the negative fields increase while the positive fields decrease the charge flow connectivity. Thus, under the negative fields, the charge flows across the system are easier to modulate while under the positive fields, the charge flows outside of the molecule are harder to modulate.

We find that the EM peak is slightly blue shifted by the negative fields and slightly red shifted by the positive fields, but the Raman intensity at the EM peak is decreased under both types of fields. In Fig. 4(c) we plot the individual contributions to the Raman intensities at the EM peaks under different electric fields. At the cluster resonance, the smaller enhancements under the negative or positive fields can be explained by the reduced $p^{\rm clu}$. The inter-fragment Raman bond is enhanced by the positive fields while reduced by the negative fields, which indicates that the positive fields increase while the negative fields decrease the charge flow connectivity across the molecule-metal interface. Thus, the decreased EM contribution under the positive fileds can be interpreted as the reduction of the local field enhancement due to the improved charge flow connectivity, which has also been shown in the comparison between the S-complex and the Vcomplex. Meanwhile, the decreased charge flow connectivity under the negative fields reduces the molecule-metal interaction and makes the charge flows in the cluster respond less effectively to the charge flow modulations in the molecule, which explains the decreased EM contribution under the negative fields. In other words, to achieve the largest EM contribution requires an optimal charge flow connectivity. Increasing or decreasing the charge flow connectivity from the optimal value will reduce the EM contribution. It should be noted again that the effect of electric fields on the geometry or the vibrational pattern is not considered here and the conclusion of the optimal charge flow connectivity is valid for a fixed geometry and vibrational pattern.

V. CONCLUSION

In this work, we have presented a frequency dependent Raman bond model which partitions the Raman intensity to interatomic charge flow modulations or Raman bonds. The frequency dependent Raman scattering is obtained using damped response theory which enables both off-resonance and resonance cases to be modeled. To understand the enhancement mechanisms of surface-enhanced Raman scattering (SERS), the Raman bond model was used to interpret the TDDFT simulations of a model system with a pyridine interacting with a small silver cluster. We show how the Raman bonds in the molecule, the inter-fragment bond, and the metal cluster are mapped to the enhancement contributions of RRS, CT, and EM respectively. The mapping quantifies the interference among RRS, CT, and EM at any incident frequency and interprets EM in electronic structure simulations as charge flow modulations in the metal. We find that the EM enhancement is strongly affected by the charge flow connectivity between the molecule and the cluster. The consistent and quantitative interpretation potentially offers new insights to the SERS applications where both CM and EM are important such as quantifying the effect of tunneling on the single molecule images obtained by tip-enhanced Raman scattering.

VI. SUPPLEMENTARY MATERIAL

Details on the color-coding of the Raman bond phases, and Raman bond patterns for the active modes of the S-complex. The excitations of S-complex near the charge transfer resonance frequency are provided. Comparison between the Raman scattering of the xx component and the orientational average Raman scattering is presented.

ACKNOWLEDGMENTS

The authors gratefully acknowledge financial support from National Science Foundation Grant CHE-1707657. Simulations in this work were conducted in part with Advanced Cyber infrastructure computational resources provided by the Institute for Cyber-Science at The Pennsylvania State University (https://ics.psu.edu/).

VII. DATA AVAILABILITY

The data that support the findings of this study are available from the corresponding author upon reasonable request.

REFERENCES

- ¹J. Langer, D. Jimenez de Aberasturi, J. Aizpurua, R. A. Alvarez-Puebla, B. Auguié, J. J. Baumberg, G. C. Bazan, S. E. J. Bell, A. Boisen, A. G. Brolo, J. Choo, D. Cialla-May, V. Deckert, L. Fabris, K. Faulds, F. J. García de Abajo, R. Goodacre, D. Graham, A. J. Haes, C. L. Haynes, C. Huck, T. Itoh, M. Käll, J. Kneipp, N. A. Kotov, H. Kuang, E. C. Le Ru, H. K. Lee, J.-F. Li, X. Y. Ling, S. A. Maier, T. Mayerhöfer, M. Moskovits, K. Murakoshi, J.-M. Nam, S. Nie, Y. Ozaki, I. Pastoriza-Santos, J. Perez-Juste, J. Popp, A. Pucci, S. Reich, B. Ren, G. C. Schatz, T. Shegai, S. Schlücker, L.-L. Tay, K. G. Thomas, Z.-Q. Tian, R. P. Van Duyne, T. Vo-Dinh, Y. Wang, K. A. Willets, C. Xu, H. Xu, Y. Xu, Y. S. Yamamoto, B. Zhao, and L. M. Liz-Marzán, "Present and future of surface-enhanced raman scattering," ACS Nano 14, 28–117 (2020).
- ²A. B. Zrimsek, N. Chiang, M. Mattei, S. Zaleski, M. O. McAnally, C. T. Chapman, A.-I. Henry, G. C. Schatz, and R. P. Van Duyne, "Single-molecule chemistry with surface- and tip-enhanced raman spectroscopy," Chem. Rev. **117**, 7583–7613 (2016).
- ³S. Yang, X. Dai, B. B. Stogin, and T.-S. Wong, "Ultrasensitive surface-enhanced raman scattering detection in common fluids," Proc. Natl. Acad. Sci. USA **113**, 268–273 (2016).
- ⁴F. Benz, M. K. Schmidt, A. Dreismann, R. Chikkaraddy, Y. Zhang, A. Demetriadou, C. Carnegie, H. Ohadi, B. de Nijs, R. Esteban, J. Aizpurua, and J. J. Baumberg, "Single-molecule optomechanics in "picocavities"," Science **354**, 726–729 (2016).
- ⁵J. Chen, W. Ding, Z. Luo, B. H. Loo, and J. Yao, "Probing single molecules and molecular aggregates: Raman spectroscopic advances," J. Raman Spectrosc. **47**, 623–635 (2016).
- ⁶A. M. Michaels, M. Nirmal, and L. E. Brus, "Surface enhanced Raman spectroscopy of individual rhodamine 6G molecules on large Ag nanocrystals," J. Am. Chem. Soc. **121**, 9932–9939 (1999).
- ⁷A. B. Zrimsek, N. L. Wong, and R. P. Van Duyne, "Single molecule surface-enhanced raman spectroscopy: A critical analysis of the bianalyte versus isotopologue proof," J. Phys. Chem. C **120**, 5133–5142 (2016).

- ⁸B. Pettinger, B. Ren, G. Picardi, R. Schuster, and G. Ertl, "Nanoscale probing of adsorbed species by tip-enhanced raman spectroscopy," Phys. Rev. Lett. **92**, 096101 (2004).
- ⁹P. Verma, "Tip-enhanced raman spectroscopy: Technique and recent advances," Chem. Rev. **117**, 6447–6466 (2017).
- ¹⁰Z. Zhang, S. Sheng, R. Wang, and M. Sun, "Tip-enhanced raman spectroscopy," Anal. Chem. **88**, 9328–9346 (2016).
- ¹¹X. Wang, S.-C. Huang, T.-X. Huang, H.-S. Su, J.-H. Zhong, Z.-C. Zeng, M.-H. Li, and B. Ren, "Tip-enhanced raman spectroscopy for surfaces and interfaces," Chem. Soc. Rev. **46**, 4020–4041 (2017).
- ¹²J. Lee, K. T. Crampton, N. Tallarida, and V. A. Apkarian, "Visualizing vibrational normal modes of a single molecule with atomically confined light," Nature **568**, 78–82 (2019).
- ¹³R. Zhang, Y. Zhang, Z. C. Dong, S. Jiang, C. Zhang, L. G. Chen, L. Zhang, Y. Liao, J. Aizpurua, Y. Luo, J. L. Yang, and J. G. Hou, "Chemical mapping of a single molecule by plasmonenhanced raman scattering," Nature 498, 82–86 (2013).
- ¹⁴E.-M. Y. e. a. Song Yuan Ding, "Electromagnetic theories of surface-enhanced raman spectroscopy," Chem. Soc. Rev. 46, 4042–4076 (2017).
- ¹⁵S.-Y. Ding, J. Yi, J.-F. Li, B. Ren, D.-Y. Wu, R. Panneerselvam, and Z.-Q. Tian, "Nanostructure-based plasmon-enhanced raman spectroscopy for surface analysis of materials," Nat. Rev. Mater. **1**, 16021 (2016).
- ¹⁶V. Amendola, R. Pilot, M. Frasconi, O. M. Maragò, and M. A. Iatì, "Surface plasmon resonance in gold nanoparticles: a review," J. Phys.: Condens. Matter **29**, 203002 (2017).
- ¹⁷K. A. Willets and R. P. Van Duyne, "Localized surface plasmon resonance spectroscopy and sensing," Ann. Rev. Phys. Chem. **58**, 267–297 (2007).
- ¹⁸H. Xu, J. Aizpurua, M. Käll, and P. Apell, "Electromagnetic contributions to single-molecule sensitivity in surface-enhanced raman scattering," Phys. Rev. E **62**, 4318–4324 (2000).
- ¹⁹M. Moskovits, "Surface-enhanced Raman spectroscopy: a brief retrospective," J. Raman Spectrosc. **36**, 485–496 (2005).
- ²⁰A. Campion and P. Kambhampati, "Surface-enhanced raman scattering," Chem. Soc. Rev. **27**, 241–250 (1998).
- ²¹D. V. Chulhai, Z. Hu, J. E. Moore, X. Chen, and L. Jensen, "Theory of linear and nonlinear surface-enhanced vibrational spectroscopies," Ann. Rev. Phys. Chem. **67**, 541–564 (2016).

- ²²L. Jensen, C. M. Aikens, and G. C. Schatz, "Electronic structure methods for studying surface-enhanced raman scattering," Chem. Soc. Rev. **37**, 1061–1073 (2008).
- ²³S. M. Morton, D. W. Silverstein, and L. Jensen, "Theoretical studies of plasmonics using electronic structure methods," Chem. Rev. **111**, 3962–3994 (2011).
- ²⁴J. R. Lombardi and R. L. Birke, "Theory of surface-enhanced raman scattering in semiconductors," J. Phys. Chem. C **118**, 11120–11130 (2014).
- ²⁵J. R. Lombardi and R. L. Birke, "Time-dependent picture of the charge-transfer contributions to surface enhanced raman spectroscopy," J. Chem. Phys. **126**, 244709 (2007).
- ²⁶J. E. Moore, S. M. Morton, and L. Jensen, "Importance of correctly describing charge-transfer excitations for understanding the chemical effect in sers," J. Phys. Chem. Lett. **3**, 2470–2475 (2012).
- ²⁷S. M. Morton and L. Jensen, "Understanding the molecule-surface chemical coupling in SERS,"
 J. Am. Chem. Soc. 131, 4090–4098 (2009).
- ²⁸R. Alvarez-Puebla, L. M. Liz-Marzán, and F. J. García de Abajo, "Light concentration at the nanometer scale," J. Phys. Chem. Lett. **1**, 2428–2434 (2010).
- ²⁹D.-K. Lim, K.-S. Jeon, H. M. Kim, J.-M. Nam, and Y. D. Suh, "Nanogap-engineerable ramanactive nanodumbbells for single-molecule detection," Nat. Mater. **9**, 60–67 (2010).
- ³⁰D.-K. Lim, K.-S. Jeon, J.-H. Hwang, H. Kim, S. Kwon, Y. D. Suh, and J.-M. Nam, "Highly uniform and reproducible surface-enhanced raman scattering from dna-tailorable nanoparticles with 1-nm interior gap," Nat. Nanotechnol. **6**, 452–460 (2011).
- ³¹K. L. Wustholz, A.-I. Henry, J. M. McMahon, R. G. Freeman, N. Valley, M. E. Piotti, M. J. Natan, G. C. Schatz, and R. P. V. Duyne, "Structure-activity relationships in gold nanoparticle dimers and trimers for surface-enhanced raman spectroscopy," J. Am. Chem. Soc. 132, 10903–10910 (2010).
- ³²H. Wang, C. S. Levin, and N. J. Halas, "Nanosphere arrays with controlled sub-10-nm gaps as surface-enhanced raman spectroscopy substrates," J. Am. Chem. Soc. **127**, 14992–14993 (2005).
- ³³W. Li, P. H. C. Camargo, X. Lu, and Y. Xia, "Dimers of silver nanospheres: Facile synthesis and their use as hot spots for surface-enhanced raman scattering," Nano Lett. **9**, 485–490 (2009).
- ³⁴J. M. McMahon, S. Li, L. K. Ausman, and G. C. Schatz, "Modeling the effect of small gaps in surface-enhanced raman spectroscopy," J. Phys. Chem. C **116**, 1627–1637 (2012).
- ³⁵N. A. Hatab, C.-H. Hsueh, A. L. Gaddis, S. T. Retterer, J.-H. Li, G. Eres, Z. Zhang, and B. Gu, "Free-standing optical gold bowtie nanoantenna with variable gap size for enhanced

- raman spectroscopy," Nano Lett. 10, 4952–4955 (2010).
- ³⁶D. A. Genov, A. K. Sarychev, V. M. Shalaev, and A. Wei, "Resonant field enhancements from metal nanoparticle arrays," Nano Lett. **4**, 153–158 (2004).
- ³⁷M. Futamata, Y. Maruyama, and M. Ishikawa, "Local electric field and scattering cross section of ag nanoparticles under surface plasmon resonance by finite difference time domain method,"
 J. Phys. Chem. B 107, 7607–7617 (2003).
- ³⁸W. Zhang, Cui, B.-S. Yeo, T. Schmid, C. Hafner, and R. Zenobi, "Nanoscale roughness on metal surfaces can increase tip-enhanced raman scattering by an order of magnitude," Nano Lett. **7**, 1401–1405 (2007).
- ³⁹J. H. Yoon, Y. Zhou, M. G. Blaber, G. C. Schatz, and S. Yoon, "Surface plasmon coupling of compositionally heterogeneous core-satellite nanoassemblies," J. Phys. Chem. Lett. **4**, 1371–1378 (2013).
- ⁴⁰R. Esteban, A. G. Borisov, P. Nordlander, and J. Aizpurua, "Bridging quantum and classical plasmonics with a quantum-corrected model," Nat Commun. **3**, 825 (2012).
- ⁴¹J. Zuloaga, E. Prodan, and P. Nordlander, "Quantum plasmonics: Optical properties and tunability of metallic nanorods," ACS Nano **4**, 5269–5276 (2010).
- ⁴²P. Liu, D. V. Chulhai, and L. Jensen, "Atomistic characterization of plasmonic dimers in the quantum size regime," J. Phys. Chem. C **123**, 13900–13907 (2019).
- ⁴³C. Readman, B. de Nijs, I. Szabó, A. Demetriadou, R. Greenhalgh, C. Durkan, E. Rosta, O. A. Scherman, and J. J. Baumberg, "Anomalously large spectral shifts near the quantum tunnelling limit in plasmonic rulers with subatomic resolution," Nano Lett. **19**, 2051–2058 (2019).
- ⁴⁴D.-J. Yang, S. Zhang, S.-J. Im, Q.-Q. Wang, H. Xu, and S. Gao, "Analytical analysis of spectral sensitivity of plasmon resonances in a nanocavity," Nanoscale **11**, 10977–10983 (2019).
- ⁴⁵S. F. Tan, L. Wu, J. K. W. Yang, P. Bai, M. Bosman, and C. A. Nijhuis, "Quantum Plasmon Resonances Controlled by Molecular Tunnel Junctions," Science **343**, 1496–1499 (2014).
- ⁴⁶R. T. Hill, J. J. Mock, A. Hucknall, S. D. Wolter, N. M. Jokerst, D. R. Smith, and A. Chilkoti, "Plasmon ruler with angstrom length resolution," ACS Nano **6**, 9237–9246 (2012).
- ⁴⁷D.-Y. Wu, J.-F. Li, B. Ren, and Z.-Q. Tian, "Electrochemical surface-enhanced raman spectroscopy of nanostructures," Chem. Soc. Rev. **37**, 1025–1041 (2008).
- ⁴⁸S. Sun and P. Wu, "Competitive surface-enhanced raman scattering effects in noble metal nanoparticle-decorated graphene sheets," Phys. Chem. Chem. Phys. **13**, 21116–21120 (2011).

- ⁴⁹R. Esteban, A. Zugarramurdi, P. Zhang, P. Nordlander, F. J. Garcia-Vidal, A. G. Borisov, and J. Aizpurua, "A classical treatment of optical tunneling in plasmonic gaps: extending the quantum corrected model to practical situations," Faraday Discuss. **178**, 151–183 (2015).
- ⁵⁰L. Zhao, L. Jensen, and G. C. Schatz, "Pyridine-Ag₂₀ cluster: A model system for studying surface-enhanced raman scattering," J. Am. Chem. Soc. **128**, 2911–2919 (2006).
- ⁵¹N. Valley, N. Greeneltch, R. P. Van Duyne, and G. C. Schatz, "A look at the origin and magnitude of the chemical contribution to the enhancement mechanism of surface-enhanced raman spectroscopy (SERS): Theory and experiment," J. Phys. Chem. Lett. **4**, 2599–2604 (2013).
- ⁵²R. L. M. Gieseking, J. Lee, N. Tallarida, V. A. Apkarian, and G. C. Schatz, "Bias-dependent chemical enhancement and nonclassical stark effect in tip-enhanced raman spectromicroscopy of co-terminated ag tips," J. Phys. Chem. Lett. **9**, 3074–3080 (2018).
- ⁵³R. L. Gieseking, M. A. Ratner, and G. C. Schatz, "Semiempirical modeling of electrochemical charge transfer," Faraday Discuss. **199**, 547–563 (2017).
- ⁵⁴R. L. Gieseking, M. A. Ratner, and G. C. Schatz, "Theoretical modeling of voltage effects and the chemical mechanism in surface-enhanced raman scattering," Faraday Discuss. **205**, 149–171 (2017).
- ⁵⁵A. T. Zayak, Y. S. Hu, H. Choo, J. Bokor, S. Cabrini, P. J. Schuck, and J. B. Neaton, "Chemical raman enhancement of organic adsorbates on metal surfaces," Phys. Rev. Lett. **106**, 083003 (2011).
- ⁵⁶A. K. Kuhlman and A. T. Zayak, "Revealing interaction of organic adsorbates with semiconductor surfaces using chemically enhanced raman," J. Phys. Chem. Lett. **5**, 964–968 (2014).
- ⁵⁷A. T. Zayak, H. Choo, Y. S. Hu, D. J. Gargas, S. Cabrini, J. Bokor, P. J. Schuck, and J. B. Neaton, "Harnessing chemical raman enhancement for understanding organic adsorbate binding on metal surfaces," J. Phys. Chem. Lett. **3**, 1357–1362 (2012).
- ⁵⁸F. W. Hilty, A. K. Kuhlman, F. Pauly, and A. T. Zayak, "Raman scattering from a molecule-semiconductor interface tuned by an electric field: Density functional theory approach," J. Phys. Chem. C 119, 23113–23118 (2015).
- ⁵⁹J. Gersten and A. Nitzan, "Electromagnetic theory of enhanced Raman scattering by molecules adsorbed on rough surfaces," J. Chem. Phys. **73**, 3023–3037 (1980).
- 60 E. C. Le Ru and P. G. Etchegoin, "Rigorous justifaction of the $|e|^4$ enhancement factor in surface enhanced raman spectroscopy," Chem. Phys. Lett. **423**, 63–66 (2006).

- ⁶¹M. Barbry, P. Koval, F. Marchesin, R. Esteban, A. G. Borisov, J. Aizpurua, and D. Sánchez-Portal, "Atomistic near-field nanoplasmonics: Reaching atomic-scale resolution in nanooptics," Nano Lett. **15**, 3410–3419 (2015).
- ⁶²J. Lee, N. Tallarida, X. Chen, P. Liu, L. Jensen, and V. A. Apkarian, "Tip-enhanced raman spectromicroscopy of co(ii)-tetraphenylporphyrin on au(111): Toward the chemists' microscope," ACS Nano 11, 11466–11474 (2017).
- ⁶³S. Trautmann, J. Aizpurua, I. Gotz, A. Undisz, J. Dellith, H. Schneidewind, M. Rettenmayr, and V. Deckert, "A classical description of subnanometer resolution by atomic features in metallic structures," Nanoscale 9, 391–401 (2017).
- ⁶⁴D. V. Chulhai and L. Jensen, "Determining molecular orientation with surface-enhanced raman scattering using inhomogenous electric fields," J. Phys. Chem. C **117**, 19622–19631 (2013).
- ⁶⁵C. C. Neacsu, J. Dreyer, N. Behr, and M. B. Raschke, "Scanning-probe raman spectroscopy with single-molecule sensitivity," Phys. Rev. B **73**, 193406 (2006).
- ⁶⁶N. Jiang, D. Kurouski, E. A. Pozzi, N. Chiang, M. C. Hersam, and R. P. V. Duyne, "Tipenhanced raman spectroscopy: From concepts to practical applications," Chem. Phys. Lett. **659**, 16–24 (2016).
- ⁶⁷N. Tallarida, J. Lee, and V. A. Apkarian, "Tip-Enhanced Raman Spectromicroscopy on the Angstrom Scale: Bare and CO-Terminated Ag Tips," ACS Nano **11**, 11393–11401 (2017).
- ⁶⁸R. Chen and L. Jensen, "Interpreting the chemical mechanism in sers using a raman bond model," J. Chem. Phys. **152**, 024126 (2020).
- ⁶⁹F. L. Hirshfeld, "Bonded-atom fragments for describing molecular charge densities," Theor. Chim. Acta **44**, 129–138 (1977).
- ⁷⁰L. Jensen, L. L. Zhao, J. Autschbach, and G. C. Schatz, "Theory and method for calculating resonance Raman scattering from resonance polarizability derivatives," J. Chem. Phys. **123**, 174110 (2005).
- ⁷¹N. Ramos-Berdullas, D. López-Carballeira, M. Mandado, and I. Pérez-Juste, "Revisiting the mechanism and the influence of the excitation wavelength on the surface-enhanced raman scattering of the pyridine-ag20 system," Theor. Chem. Acc. **134**, 60 (2015).
- ⁷²L. Jensen, J. Autschbach, and G. C. Schatz, "Finite lifetime effects on the polarizability within time-dependent density-functional theory," J. Chem. Phys. **122**, 224115 (2005).
- ⁷³G. K. Laura Gagliardi, Roland Lindh, "Local properties of quantum chemical systems: The loprop approach," J. Chem. Phys. **121**, 4494–4500 (2004).

- ⁷⁴E. J. Baerends, T. Ziegler, A. J. Atkins, J. Autschbach, D. Bashford, O. Baseggio, A. Bérces, F. M. Bickelhaupt, C. Bo, P. M. Boerritger, L. Cavallo, C. Daul, D. P. Chong, D. V. Chulhai, L. Deng, R. M. Dickson, J. M. Dieterich, D. E. Ellis, M. van Faassen, A. Ghysels, A. Giammona, S. J. A. van Gisbergen, A. Goez, A. W. Götz, S. Gusarov, F. E. Harris, P. van den Hoek, Z. Hu, C. R. Jacob, H. Jacobsen, L. Jensen, L. Joubert, J. W. Kaminski, G. van Kessel, C. König, F. Kootstra, A. Kovalenko, M. Krykunov, E. van Lenthe, D. A. McCormack, A. Michalak, M. Mitoraj, S. M. Morton, J. Neugebauer, V. P. Nicu, L. Noodleman, V. P. Osinga, S. Patchkovskii, M. Pavanello, C. A. Peeples, P. H. T. Philipsen, D. Post, C. C. Pye, H. Ramanantoanina, P. Ramos, W. Ravenek, J. I. Rodríguez, P. Ros, R. Rüger, P. R. T. Schipper, D. Schlüns, H. van Schoot, G. Schreckenbach, J. S. Seldenthuis, M. Seth, J. G. Snijders, M. Solà, S. M., M. Swart, D. Swerhone, G. te Velde, V. Tognetti, P. Vernooijs, L. Versluis, L. Visscher, O. Visser, F. Wang, T. A. Wesolowski, E. M. van Wezenbeek, G. Wiesenekker, S. K. Wolff, T. K. Woo, and A. L. Yakovlev, "ADF2018, SCM, Theoretical Chemistry, Vrije Universiteit, Amsterdam, The Netherlands, https://www.scm.com," (2018).
- ⁷⁵G. te Velde, F. M. Bickelhaupt, E. J. Baerends, C. Fonseca Guerra, S. J. A. van Gisbergen, J. G. Snijders, and T. Ziegler, "Chemistry with adf," J. Comput. Chem. **22**, 931–967 (2001).
- ⁷⁶A. D. Becke, "Density-functional exchange-energy approximation with correct asymtotic-behavior," Phys. Rev. A **38**, 3098–3100 (1988).
- ⁷⁷J. P. Perdew, "Density-functional approximation for the correlation energy of the inhomogeneous electron gas," Phys. Rev. B **33**, 8822–8824 (1986).
- ⁷⁸E. van Lenthe, E. J. Baerends, and J. G. Snijders, "Relativistic regular two-component hamiltonians," J. Chem. Phys. **99**, 4597–4610 (1993).
- ⁷⁹"The pymol molecular graphics system, version 1.2r3pre, schrödinger, llc." (2019).
- ⁸⁰L. Silberstein, "L. molecular refractivity and atomic interaction. ii," Philos. Mag. **33**, 521–533 (1917).
- ⁸¹M. Osawa, N. Matsuda, K. Yoshii, and I. Uchida, "Charge transfer resonance raman process in surface-enhanced raman scattering from p-aminothiophenol adsorbed on silver: Herzberg-teller contribution," J. Phys. Chem. **98**, 12702–12707 (1994).
- ⁸²J. R. Lombardi, R. L. Birke, L. A. Sanchez, I. Bernard, and S. C. Sun, "The effect of molecular structure on voltage induced shifts of charge transfer excitation in surface enhanced raman scattering," Chem. Phys. Lett. **104**, 240–247 (1984).

⁸³C. Chenal, R. L. Birke, and J. R. Lombardi, "Determination of the degree of charge-transfer contributions to surface-enhanced Raman spectroscopy," ChemPhysChem **9**, 1617–1623 (2008).